# A Novel Approach for the Simulation of *Xenopus laevis* Tail Regeneration

A thesis submitted by

Zachary Taylor Serlin

In partial fulfillment of the requirements for the degree of

Master of Science

In

Mechanical Engineering

Tufts University

May 2016

Adviser: Dr. Jason Rife
Committee Member: Dr. Behrouz Abedian
Cross-Department Committee Member: Dr. Michael Levin

# Abstract

A framework for predictively linking cell-level signaling with larger scale patterning in regeneration and growth has yet to be created within the field of regenerative biology. If this could be achieved, regeneration (controlled cell growth), cancer (uncontrolled cell growth), and birth defects (mispatterning of cell growth) could be more easily understood and manipulated. This thesis looks to create a framework to predict macroscopic regenerative morphology using level-set methods, a cellular-based control scheme, and a morphogen-based positioning field. The key contribution is defining velocity models for the control scheme that bridge microscopic and macroscopic scales. The novel control scheme proposed uses three control mechanisms to collectively mimic biological regeneration. Application to the simulation of *Xenopus laevis* tail regeneration suggests the utility of the proposed methods.

# Acknowledgements

I would like to thank my committee members. First and foremost my advisor Professor Jason Rife, who has fostered an upbeat, inspiring, and welcoming environment that provides students with direction and guidance while promoting freedom of discovery and innovation. He is a brilliant educator whose love of discovery, passion for science, and cheerful attitude are infectious. Next, I would like to thank Professor Michael Levin for providing biological background for this work, being extremely welcoming and responsive to questions, and taking the time to discuss the direction of this work throughout its development. His unique prospective and experience has been invaluable. Finally, I would like to thank Professor Behrouz Abedian for taking the time to serve on this committee and for providing me guidance throughout my career at Tufts. Since my freshmen year, his guidance and prospective has been greatly appreciated.

I would next like to thank Tufts University and the Mechanical Engineering Department, specifically Lorin Polidora and Megan Dauphinais, for all of their help and support. From organizing paperwork submissions to keeping track of important dates, the ME office was always there to help. I would also like to extend my thanks to Zilia Munguia for scheduling advisor meetings and being extremely flexible when rescheduling.

I would like to extend my appreciation to all of my friends, fellow students, and peers at Tufts. Many of you I have known since freshmen year and I do not know where I would be without your constant support. I would like to

thank the members of the CRISP and ASAR labs, both current and former. You have taught me a great deal and have provided invaluable feedback throughout the years. Thank you to all of my classmates who studied with me, worked on problem sets, spent long nights in Blake (sometimes until the police kicked us out), practiced presentations, became closer friends. You have made my Tufts experience truly memorable.

Finally, I would like to extend a huge thank you to my family. I want to thank my parents for always being there with support, love, and advice that has gotten me through the years. I don't know where I would be without them and I want to thank them really for everything they have done for me.

# Table of Contents

# List of Tables

# List of Figures

# Nomenclature

Table 1: Variable Definitions

| Symbol | Description |
|---|---|
| $x$ | Anterior/Posterior Coordinate |
| $y$ | Dorsal/Ventral Coordinate |
| $\phi$ | Level Set Scalar Value |
| $\Gamma$ | Boundary Contour |
| $\mathbf{v}(x,y)$ | Velocity Field |
| $S(x,y,t)$ | Scalar Field Source Term |
| $\mathbf{n}$ | Local Unit Normal |
| $F$ | Magnitude of Local Normal |
| t | Time |
| $P$ | Patterning Control |
| $I$ | Isometric Control |
| $K$ | Smoothing Control |
| $\phi_{ref}$ | Global Reference Map |
| $e(x,y,t)$ | Error Term at Each Point |
| $C_p$ | Patterning Control Gain |
| $F_{max}$ | Maximum Growth Speed |
| $d$ | Distance From Contour |
| $F_V$ | Isometry Growth Speed |
| $V_{tot}$ | Total Organism Volume |
| $V_{pat}$ | Patterning Region Volume |
| SA | Organism Surface Area |
| $C_{GC,\text{nom}}$ | Nominal Cellular Growth Rate |
| $C_{GC,\text{max}}$ | Maximum Cellular Growth Rate |
| $\kappa$ | Curvature of Scalar Field |
| $C_\kappa$ | Smoothing Control Gain |
| $\rho$ | Diffusion Field Concentration |
| D | Diffusion Coefficient |
| C | Decay Coefficient |
| S | Diffusion Source |
| n | Time Step |

# A Novel Approach for the Simulation of *Xenopus laevis* Tail Regeneration

## Chapter 1 Introduction

### Section 1.1 Motivation

This thesis describes a new approach to simulating *Xenopus laevis* tail regeneration.

The overarching goal behind this work is to glean a deeper understanding of regeneration, growth, and patterning mechanics through simplified models. The regenerative and developmental biology community has interest in these models to fill a void in current predictive capabilities of regeneration and growth. Many models exist for microscopic cell communication and growth [1]–[5] but the underlying concept behind many of these models is interactions of individual cells. Each cell has a basic control law to create these agent-based or cellular automata models [1], [6], [7]. These models are effective at modeling clusters of individual cells but ultimately struggle to represent larger structures. They require a large number of calculations per cell and would be unwieldy and time consuming to implement at the macroscopic level (limbs, organs, and even organisms). Beyond computation hurdles, when these models are taken to even the mesoscale they do not deal with voids, irregularities, and unrealistic features and therefore often develop biologically unrealistic features [8]. Some models

have been effective at predicting cell differentiation at the macroscopic level using regulatory network models and top-down approaches [9], [10]. These models look at morphology and cell differentiation but often do not bridge multiple scales. Few models attempt to model macroscopic *Xenopus* tail regeneration. Most of these models are still based on micro-scale interactions and model large clusters of cells as individual cells to reduce complexity. This results in limited accuracy of pattern emergence [5].

## Section 1.2 Proposed Model

A novel approach to simulating *Xenopus laevis* is presented in the following chapters. The approach consists of software modules that are intertwined to mimic biological cell growth, patterning, and navigation. The first module is a growth model that creates the basic physics of the simulation using level set methods. The second module is a novel control scheme that mimics both regenerative and nominal growth by manipulating boundary velocities in the level set field. This scheme contains three control regimes using patterning control for regenerative bud patterning and regeneration, isometric control for volumetric growth, and smoothing control to reduce curvature and reinforce a minimum feature size in the level set field. The third module is a navigation model that mimics cellular communication, allowing cells to estimate their position within the regenerating structure. The future utility of this simulation is to ultimately better understand the biological mechanisms that relate microscopic, cell-level behavior to macroscopic, organism-level growth.

## Section 1.3 Contributions

For the most part, the tools described in this dissertation to simulate *Xenopus laevis* are not new. What is unique about our simulation is the introduction of new control laws that simulate the motion of the outer boundary of the organism during growth and regeneration. These control laws are carefully formulated to model how microscopic cell behavior (e.g. cell division) impacts morphogenesis at a macroscopic scale.

**Contribution 1: Created a set of novel boundary velocity control laws that link micro-scale cell behavior to macro-scale morphogenesis for use in a simulation of regeneration.**

A model for biological growth and regeneration is created using novel boundary velocity control laws. Level set methods create a field for the boundary motion to take place; while, the control laws manipulate boundary velocities to simulate outer organism boundary motion.

This model bridges an existing gap between current micro and macro scale models by abstracting individual cell behavior into collective macroscopic phenomena using the control laws. Current micro-scale models have difficulties modeling even mesoscale features due to their high level of detail and complexity. At the same time, current macro-scale models are either inaccurate or have a low level of detail due to their extreme levels of abstraction. The model proposed here solves these issues by starting from simple cell behaviors (like in the micro-scale models) and merging them with existing level set methods for macro-scale boundary propagation.

These boundary velocity control laws are a new tool for the regenerative biology community to use in the search for deeper understanding of regeneration, growth, and patterning. Because they bridge the mesoscale gap, they can directly link the functions of individual cells to emergent patterning.

*Contribution 1a: Modeled the boundary velocity using three bioinspired control laws: isometric control, patterning control, and smoothing control.*

To model microscopic mechanisms of regeneration and growth, the novel controller is implemented using three control laws. Each law (or regime) represents a different aspect of cell behavior. The first regime, patterning control, alters tail morphology to regenerate tail shape to mimic regenerative cell growth. The second regime, isometric control, alters tail size while preserving shape to mimic natural cell division. The finally regime, smoothing control, reduces curvature in the field to smooth body shape which mimics the collective cohesiveness of cells. These regimes work in concert to predict regenerative morphology.

*Contribution 1b: Simulated Xenopus laevis tail regeneration to test qualitative functionality of proposed control model.*

*Xenopus laevis* was chosen as the animal of focus for its simplicity, regenerative capabilities, and large achieve of previous experimentation. The control model is tested with four case studies. Each study looks to test a different control law and ultimately determine if the model as a whole qualitatively makes sense. The control model can be extended to regenerate any closed contour

morphology (i.e. hands, limbs, or organs). This makes it a powerful tool for general regeneration research in the future.

In support of the primary contribution, we published the first paper on modeling regenerative morphology using a level set methodology and the new velocity control model. To our knowledge, a control scheme has never before been used in level set methods to predict macroscopic biological patterning or regeneration. This paper will hopefully disseminate this technique into the broader regenerative and developmental biology community.

**Contribution 2: Evaluated the practicality of a diffusion-based model for cell navigation.**

A model is proposed to simplify complex cell communication into the diffusion of signaling chemicals throughout the tail structure. This is done using a classical diffusion model with discreet sources and a distributed sink. Two chemical species, in perpendicular orientations, are independently simulated to supply each cell with a unique concentration internal to the regenerating morphology. This unique concentration can be directly linked to a unique position. This model is, admittedly, a logical extension of existing techniques (i.e. other morphogen gradient models); however, in the future this model will provide position estimates to the control scheme during regeneration.

## Section 1.4 Thesis Overview

The remainder of the thesis comprise two main technical chapters and a conclusion.

Chapter 2 describes both the level set module and the boundary velocity control module used in the growth model. These two modules are tightly linked and therefore presented together. The chapter begins by presenting a background and methodology for the level set method and the control laws. The results of the simulation verification are then presented and analyzed to check the functionality of the simulation. The chapter is concluded by discussing the results and possible future work.

Chapter 3 describes a morphogen model to estimate internal cell position. It begins by presenting a background and methodology for creating two dimensional diffusion fields. The implementation and results of the simulation are then presented and analyzed.

Chapter 4 concludes the thesis. It looks back at the three modules of the overall simulation and reiterates the contributions made in the thesis. It then looks at possible areas of future work.

# Chapter 2 A Level Set Approach to Regeneration [1]

## Section 2.1 Abstract

A framework for predictively linking cell-level signaling with larger scale patterning in regeneration and growth has yet to be created within the field of regenerative biology. If this could be achieved, regeneration (controlled cell growth), cancer (uncontrolled cell growth), and birth defects (mispatterning of cell growth) could be more easily understood and manipulated. This chapter looks to create a key part of this preliminary framework by using level set methods and a cellular control scheme to predict macroscopic regenerative morphology. This simulation specifically looks at *Xenopus laevis* tail regeneration, and uses three control regimes to collectively mimic biological regeneration. The algorithm shows promise in creating an abstracted model to predict cell patterning on a macroscopic level.

[1] This Chapter was published under the title "A Level Set Approach to Simulating *Xenopus laevis* Tail Regeneration" at the ALIFE XV conference. The only change made to the text was a substitution of the words *this chapter* for *this paper*. The text is otherwise identical.

## Section 2.2 Introduction

If the control of cell growth and tissue patterning can be better understood, cancer (uncontrolled cell growth), birth defects (mispatterning), and organ regeneration (cell growth harnessed toward the repair of complex organs) could be more easily manipulated. While the molecular mechanisms of cellular control are increasingly understood, the field lacks frameworks for predictively linking cell-level signals to large-scale pattern controls. This chapter looks to leverage methods from continuum mechanics to provide new tools for modeling the control of cell growth and patterning. To do this, regeneration in tadpole tails is modeled as an iteration between two processes. The first process is a control scheme, which decides where and when tissue should grow or shrink. The second process is a growth model that describes changes in tissue morphology due to cell division, motion, and growth.

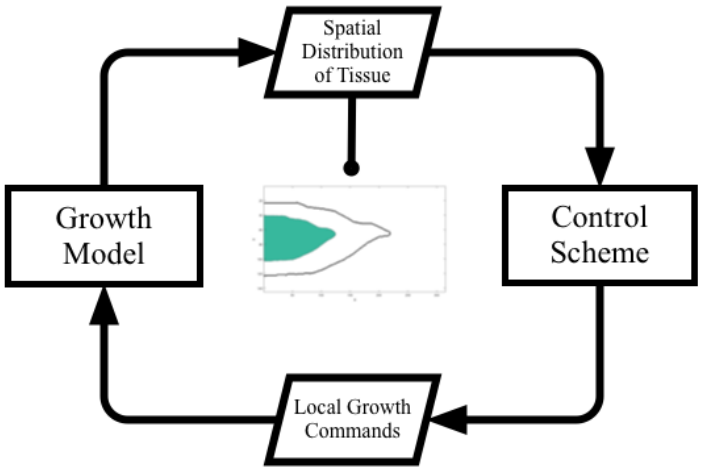


Figure 2: Two-process system model. The control scheme creates local growth commands, which the growth model uses to outputs the spatial distribution of tissue.

One challenge in modeling regeneration and tissue growth is relating the large (organism) scale to small (cell) scales. Traditionally, as the scale of the organism increases, so does the computational expense of modeling its smallest features and interactions. The average human is composed of 37.2 trillion cells – an unrealistic number of cells and interactions to model [11]. Our proposed method is advantageous because it treats tissue as a continuum, blurring the boundaries between individual cells. This approach avoids the problem of managing cells as individual agents, which like marbles on a Chinese checkers board, would need to be shuffled to open spaces to make room for new marbles.

What we describe is the difference between tracking individual agents and tracking the motion of bulk material through a fixed volume of space. Two types of mathematical thinking exist to distinguish these types of phenomena. The first approach is Lagrangian, meaning cells are tracked on an individual basis. Such a method allows cells to operate on their own growth rules and is commonly used in biological growth modeling [6], [12]. Lagrange models often suffer morphologically from internal voids because the individual "cells" cannot directly organize in a manner that preserves contact without overlapping. The second approach is Eulerian, meaning it focuses on the space through which particles move. Eulerian approaches are classically employed in modeling fluid flow and heat transfer [13], [14]. Such methods have not been widely used to model tissue

growth and patterning; however, they offer great promise to capture the effects of microscopic phenomena interacting across macroscopic domains.

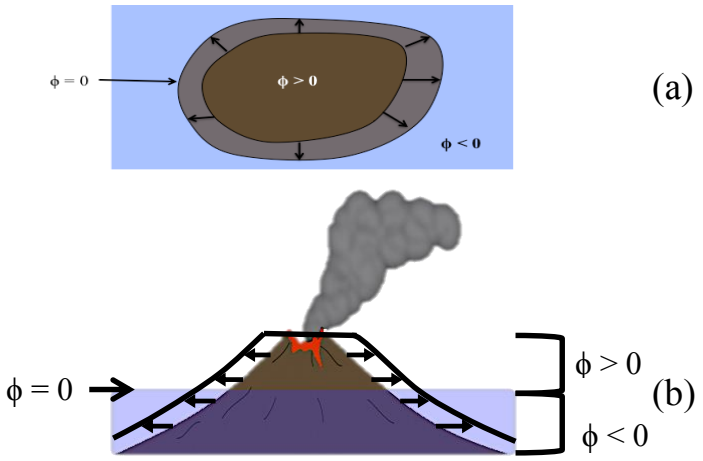


Figure 2: (a) Top view of the volcanic island erupting – arrows indicate boundary movement. (b) Front view of the volcanic island describing the same boundary movement. Elevation above sea level is indicated by the variable ϕ. Addition of volcanic material increases elevation and translates directly to change in island circumference.

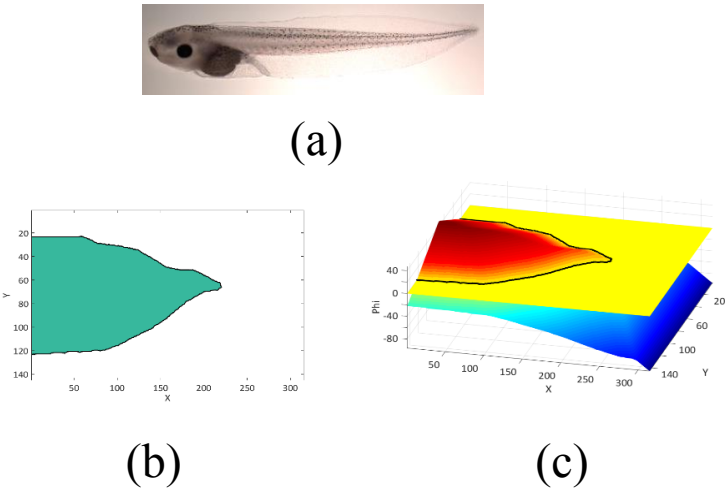


Figure 3: Level Set Scalar Field Derivation (a) *Xenopus laevis* at stage 42. (b) A 2D view of the tail representation. This represents the morphology of the tail and is the zero level set contour of the scalar field. (c) A 3D representation of the level set field. The flat plane is the zero level set. Above that plane represents material inside the body; while, the section below that plane is outside the body. The black line represents the current zero contour.

Our proposed model uses an Eulerian approach based on the level-set method. Level sets use a modified mass balance to describe a moving boundary, such as the interface between an organism and the surrounding medium. Level set methods are used to model crystal growth and combustion, as well as for computer vision and microchip fabrication [13]–[16]. Level set methods have also seen some use in biological modeling [17] although not to our knowledge in a closed-loop feedback scheme for patterned growth as illustrated in Figure 1.

Level set methods use a scalar field to describe a moving boundary. The boundary is at the zero values of the scalar field and motion of the boundary is determined by assigning a speed at each point. The speed function is ultimately what controls the development of the boundary. For this biology-motivated application, we propose a speed function consisting of three main components: isometric control, patterning control, and smoothing control.

This chapter uses level sets to simulate the regeneration of the amputated tail of a *Xenopus laevis* tadpole. *Xenopus* is a simple vertebrate that regenerates its tail until early in its life cycle, through stage 52 or 53 [18]. This makes *Xenopus* ideal for modeling patterning growth, and regeneration in particular, across a macroscopic scale. In this work, we conceptualize regeneration as growth that restores animal morphology back to a "reference" shape. Our particular approach will assume that a global reference map is available and that control laws act by setting growth rate based on the distance of the organism boundary from the reference. In fact, it is not critical as to whether an actual reference "map" might exist in an animal system [19] or whether the "map" is an emergent pattern that

results from local control decisions [5], [20]–[22]. On the simulation scale, both mechanisms are functionally equivalent.

In the following sections, this chapter will detail methods used to implement the growth model and the control scheme. The chapter will then go into detail on the simulation used to assess these models. Finally, we will present results, conclusions, and future work.

## Section 2.3 Methods

### Section 2.3.1 Level Set Analogy

Level set methods were originally created to model combustion and two-phase flow [15]. A level set can be conceived as a geographic contour map, where each level set is an elevation contour that consists of the set of points at a particular elevation. These contours may change over time if geography changes. By following a particular contour in time, it is possible to model the motion of an interface (e.g. a flame front in combustion or a liquid-gas interface in two-phase flow).

To make the geographic analogy more concrete, consider a particular case – a volcanic island rising out of the ocean (Figure 2). In this example, we will track *sea level* over time, as this elevation marks the interface between the island and the ocean. As a volcanic eruption takes place and adds material over the entire island, the island's elevation map will evolve both on the land side (topography) and on the ocean side (bathymetry). The addition of new material will cause the island to grow, such that the sea-level elevation contour pushes

outward as shown in Figure 2. Erosion would garner the opposite effect – sharp features would be worn down, shrinking the boundary. In Figure 2, the elevation is denoted by the scalar $\phi$. The interface between land and water is denoted by the sea-level contour, with $\phi = 0$.

This geographic concept can be extended to biological modeling. In this chapter, we consider a two-dimensional model of the *Xenopus* tail. In our model, the *x* coordinate corresponds to the anterior-posterior direction, the *y* coordinate to the dorsal-ventral direction, and the lateral direction is not modeled. The level set field $\phi(x,y)$ is now used to represent distance away from the outer surface of the organism. The contour that represents the outer surface of the organism is labeled $\Gamma$ and represents the set of all points where $\phi = 0$. Moving inside the organism, the distance-from-contour is measured as positive and so $\phi$ is set positive inside the organism. By contrast, $\phi$ is set negative outside the organism. This mathematical approach lets us track the motion of the outer surface of the organism through space as the organism grows in time. An illustration of this concept is shown in Figure 3, which depicts a section of the *Xenopus* tail. A photo of the *Xenpous* tadpole, in Figure 3(a), shows the tail prior to amputation. The outer tail surface can be identified and used to generate a binary image, as shown in Figure 3(b), where the green region indicates the interior of the organism and the light region indicates the exterior. This tail region can also be viewed as a level set field, shown in three-dimensions in Figure 3(c). The height of the field indicates the distance of each (*x*,*y*) point from the outer surface of the organism.

**Section 2.3.2 Growth Model**

This section describes the level set equations we used to model organism growth. Begin by identifying the outer surface of the organism in a Cartesian space described by coordinates *x* and *y*. In two-dimensions, the outer surface of the animal is a contour, which we label Γ as shown in Figure 3(b). Now construct a scalar field $\phi(x,y)$ that represents distance from the contour Γ, with values increasing interior to the organism ($\phi > 0$) and decreasing exterior to the organism ($\phi < 0$). In order to represent distance, note that the gradient of this scalar field must be one at all points where the slope of the field is continuous. Slope discontinuities appear only at the center of the field, where points are equidistant from multiple sections of the Γ contour, as illustrated by the ridge that appears along the midline of the tail, as illustrated in Figure 3(c).

To model growth, we evolve the scalar field $\phi$ over time. As time advances, the level set is propagated using a velocity field **v**(x,y), where the velocity vector is specified at every point in the field. The magnitude *F* of the velocity vector will be set by the control scheme, as described below. As the control scheme transform the scalar field, the outer surface of the organism Γ moves in time, representing organism growth.

The following equation governs the time dynamics of the scalar field $\phi(x, y, t)$.

$$\frac{D}{Dt}\phi = S(x, y, t) \quad (1)$$

Here the full derivative of the scalar ϕ is related to a source term *S*. The source term allows for the production of new material (or the destruction of old material) at every point in the field. Where the source term is zero, there is no change in the total amount of material present; in other words, ϕ is conserved in the absence of a source term. Equation (1) is a classical conservation law from continuum mechanics, as might be used to model the conservation of mass, momentum, or energy [23].

The full derivative is linked to velocity **v** through the following equation.

$$\frac{D}{Dt}\phi(x,y,t) = \phi_t + \nabla\phi \cdot \mathbf{v} \tag{2}$$

This equation, obtained from standard calculus using the chain rule, uses the notation $\phi_t$ to identify the partial derivative of $\phi$ with respect to time and the notation $\nabla\phi$ to identify its spatial gradient. In this work, $\phi$ contours are assumed always to move outward in the direction normal to each existing contour. The local unit normal to each contour is defined by the gradient:

$$\mathbf{n} = \frac{\nabla\phi}{\|\nabla\phi\|} \tag{3}$$

The velocity vector can be written in terms of a magnitude term *F* multiplied by this local normal.

$$\mathbf{v} = -F\mathbf{n} \tag{4}$$

The negative sign is introduced here, so that a positive speed *F* corresponds to organism growth (toward lower values of $\phi$). A field in which velocity is locally normal to the contour is shown in Figure 4.

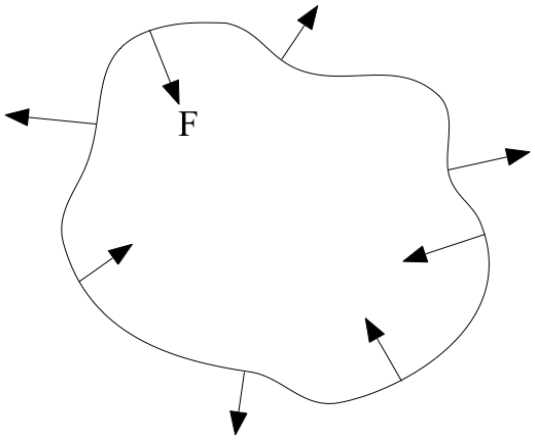


Figure 4: Velocity normal to level set contour. All movement is normal to each point on the contour. Only the magnitude of *F* determines contour movement.

Substituting equation (4) into equation (2) gives

$$\frac{D}{Dt}\phi(x,y,t) = \phi_t - F\|\nabla\phi\| \tag{5}$$

Recalling that the gradient is equal to one at all points where it is defined, the full derivative becomes

$$\frac{D}{Dt}\phi(x,y,t) = \phi_t - F \tag{6}$$

where the gradient $\nabla\phi$ is continuous. To avoid issues with the gradient being undefined at some locations (at cusps and ridges in the $\phi$ field), the velocity magnitude *F* is restricted to be zero at these locations. Thus, by combining equations (1) and (6), we obtain the following equation to describe the change in the level set field $\phi$ at each point and at each moment in time.

$$\phi_t = \begin{cases} F + S, & \nabla\phi \; defined \\ S, & elsewhere \end{cases} \tag{7}$$

Because this equation for propagating the $\phi$ field behaves differently in regions where the gradient is either continuous or not, it is natural to decompose our solution approach into two parts. In the first part of the solution, we update the field at each time step assuming that the source term is negligible. For this step we use a first-order discretization of equation (7).

$$\phi(t+\Delta t) = \begin{cases} \phi(t) + F\Delta t, & \nabla\phi \; defined \\ \phi(t), & elsewhere \end{cases} \tag{8}$$

Assuming a negligible source term is reasonable over short time periods; however, over longer periods neglecting the source term rapidly degrades the assumption that the gradient is unity magnitude (where defined), since a source should exist at peaks and ridges (as in the Volcano example of Figure 2). As such, the source term must be taken into account somehow.

To account for the source term, we use a process called reinitialization [13], [14], [24], [25]. Reinitialization serves two purposes; it forces the non-boundary region to have a gradient of one, and it implicitly adds material to the whole field to maintain the field's shape. In particular, we use a process called a narrowband reinitialization [16]. The narrowband solution assumes that the location of the zero-contour $\Gamma$ is predicted accurately. The solution domain is then divided into two regions: a region near the zero-contour (the *interface* region) and the region farther from the zero-contour (the *far field*). Values of $\phi$ in the interface region are preserved; values in the far field are replaced by computing the distance of each location from the zero contour. Although this process does not correct the gradient inside the interface region, the far field values effectively

introduce a boundary condition that drives the slope in the interface region back toward its correct magnitude (of one). This narrowband approach is numerically robust and has been used extensively in other applications of the level set method [16].

A practical issue is that the approximations introduced by narrow banding can affect the accuracy of the prediction of the zero-contour Γ. A balance must be struck however between giving the zero-contour freedom of movement and constraining the field to a gradient of one. For this reason, reinitialization is not necessarily performed at every time update. In our method, we used a boundary width of 2 pixels on either side of the Γ contour and performed reinitialization at a rate of once per 20 time steps.

In summary, the key idea of the growth model is that a velocity field can be assigned to every point in space, allowing the organism surface Γ to be grown without knowing the precise location of that surface. This property is in turn useful because it permits the simulation of a smooth, continuous boundary using a relatively coarse grid.

**Section 2.3.3 Control Scheme**

In this section we describe a control law that can be used to in conjunction with the level set methodology to define organism shape during regeneration. The control law defines a velocity field at every point in the simulation domain. As described by equation (4), the velocity is locally normal to contours of constant $\phi$. The velocity magnitude $F$ is set by the control described in this section. Specifically, $F$ is a summation of three terms, which are assumed to act

independent of each other. These terms include patterning control *P*, isometric control *I*, and smoothing control *K*. Each term models a distinct aspect of biological growth. It is important to note, however, that the models are phenomenological in nature and are not derived directly from detailed data sets. Taken together, the three terms sum to give *F*.

$$F = P + I + \mathrm{K} \tag{9}$$

All terms in this equation are functions of 2D space and time.

***Patterning Control*:** Patterning control, *P*, is the key term for this chapter as it shapes morphology by enabling local growth. The idea is that local cell-level actions may trigger tissue deterioration or growth in a small region (as at the regeneration site or *blastema* in an amputated *Xenopus* tail [26]). These local actions are responsible for regeneration and also for shape changes that occur during normal growth. Furthermore, this local activity counteracts disturbances, constantly adding or removing tissue to maintain an appropriate organism shape under varying environmental conditions. In principle, a failure of local patterning might result in uncontrolled growth (i.e. cancer).

In our simulation, we assume that patterning growth is active for cells that are near the organism surface Γ but that are not at a desired location. For simplicity, we use a global reference map $\phi_{\mathrm{ref}}$, which is scaled to the current width of the simulated tail. From this map, we derive an error *e* at each point in the simulation domain.

$$e(x, y, t) = \phi_{ref}(x, y, t) - \phi(x, y, t) \tag{10}$$

The error for a given element of tissue represents the difference between its desired and actual distance from the organism surface. The error term is limited to a maximum value, $e_{max}$, to reflect a threshold where the cells are so far from their target that they grow at a maximum rate. In the region near the organism surface, the patterning speed is set to be proportional to the error.

This proportionality is capped, however, to reflect a maximum cellular growth rate, which is slightly faster than nominal, isometric growth. The maximum speed $F_{max}$ is related to the maximum cellular growth rate $C_{GC,max}$.

$$F_{max} = \frac{V_{pat}}{SA} C_{GC,max} \tag{11}$$

Here the variable *SA* represents the surface area (which in 2D is the length of the contour where $\phi = 0$). The variable $V_{pat}$ represents the volume of tissue that is active in patterning and is proportional to $V_{tot}$. The result is that patterning growth is nonzero only in the active region; in this region patterning growth is nominally proportional to error, subject to saturation if the growth rate becomes too large or too small.

$$P = \begin{cases} F_{max} \frac{e}{e_{max}} & |e| < e_{max} \text{ and } 0 < \phi \leq d \\ F_{max} \text{sign}(e) & |e| \geq e_{max} \text{ and } 0 < \phi \leq d \\ 0 & otherwise \end{cases} \tag{12}$$

***Isometric Control*:** Our simulation uses an isometric control term *I* to allow for growth that is organism wide (as compared to patterning growth which is local). We assume that this growth occurs at the same rate throughout the entire organism, such that the organism maintains its shape when only *I* is active.

Isometric growth is, in fact, a nominal behavior for some organisms such as the flatworm. When food resources are plentiful, the flatworm grows uniformly in all directions; when the flatworm is starved it shrinks uniformly in all directions [27]. In *Xenopus* tadpoles, by contrast, some changes in shape occur as the organism grows [18], [21], [28], and so nominal growth combines some aspects of isometric control *I* with patterning control *P*.

The isometric control term has a uniform value of $F_V$ everywhere in the simulation domain when the term is active.

$$I = F_V \tag{13}$$

The isometric model represents constant cellular growth with time, meaning the boundary velocity must increase in time (as the volume to surface area ratio increases). To account for this, the growth speed $F_v$ is computed as

$$F_V = \frac{Vtot}{SA} C_{GC,nom} \tag{14}$$

Here $V_{tot}$ represents the total volume of the organism (or in this 2D simulation, the area of the tail). The rate $C_{GC,nom}$ represents the rate of cellular growth (mitosis), which is modeled to be uniform in space . For our simulations we assume that sufficient resources are available to the organism to maintain a nominal growth rate $C_{GC,nom}$ that is constant in time.

***Smoothing Control*:** The final term of the speed function is a smoothing control term K designed to eliminate sharp features (e.g., corners created by amputation) or to eliminate tissue filaments that might (by random chance) begin to develop as

extensions of the organism surface. This term essentially regularizes the organism surface to maintain smoothness. The specific mechanism for performing smoothing is to introduce a perturbation to the growth rate that is proportional to the local curvature $\kappa$ of the $\phi$ contours. The constant of proportionality is $C_\kappa$.

$$K(x, y, t) = C_\kappa \kappa(x, y, t) \tag{15}$$

This concept for smoothing has been employed in other applications of level set methods, as described by [14], [16], [24], [25]. In our biological application, the curvature term not only eliminates spurious features; it is meant to prevent the formation of holes and discontinuities that are not represented in the reference map.

By definition, curvature in a level set is the spatial derivative of normal vectors along a contour. The more rapidly the contour changes direction, the higher will be its curvature. Mathematically, curvature can be written

$$\kappa = \nabla \cdot \mathbf{n} \tag{16}$$

where the normal vector **n** is defined by equation (3) above.

Each control regimes can be linked directly to micro scale cell behavior that impacts macro scale morphology. Patterning control begins by considering a maximum growth rate of individual regeneration, multiplies that growth by the number of patterning cells, and then distributes that growth along the growing boundary. Similarly, isometric control begins by considering the natural growth rate of cell division, multiples that growth by the cells in the tail, and distributes this growth over the body boundary by dividing by the surface area of the tail.

Smoothing control is not as simply related to cell growth, but instead represents cohesiveness in the cellular matrix by minimizing areas of high curvature or irregularity.

There are three main constants that control the behavior of this simulation. Patterning control is modulated by $C_{GC,max}$, the maximum rate of regenerative growth. For this thesis, this value is found by fitting simulation results (tail length per time) to the regeneration series shown in Reid et. al. [29]. More specifically, the length per time curve of the simulation is aligned with the days 5, 9 and 12 post amputation lengths. This value is found to be 0.02. Isometric control is modulated by $C_{GC,nom}$, the nominal growth constant. This value is found by analyzing the length per time growth rate of undamaged tadpoles, shown in the normal table of Xenopus laevis [30]. This value is found to be 0.00075. The final constant, $C_{\kappa}$, controls the intensity of smoothing control. It is tuned by testing the simulation at steady state. This achieved by setting isometric control to zero and starting the simulation at its reference morphology. The simulation is then qualitatively evaluated to check that the tail is not eroded with time (meaning patterning and smoothing controls balance). This value is found to be 0.001. These three control parameters, for this thesis, are tuned to *Xenopus laevis* growth. It is important to note however, that these values may vary for different animals and different morphologies.

**Section 2.3.4 Implementation**

Each time step is represented by a single iteration of the main loop shown in Figure 5. In general, the simulation is allowed to run for 15,000 time steps, but this number must be adapted to grid resolution and control coefficients.

The level set $\phi$ is stored as a two-dimensional array on a Cartesian x-y grid. In this simulation the size of the grid was 301 pixels (anterior-posterior) and 135 pixels (dorsal-ventral). Two extra cells pad the field on each edge to simplify gradient and curvature calculations.

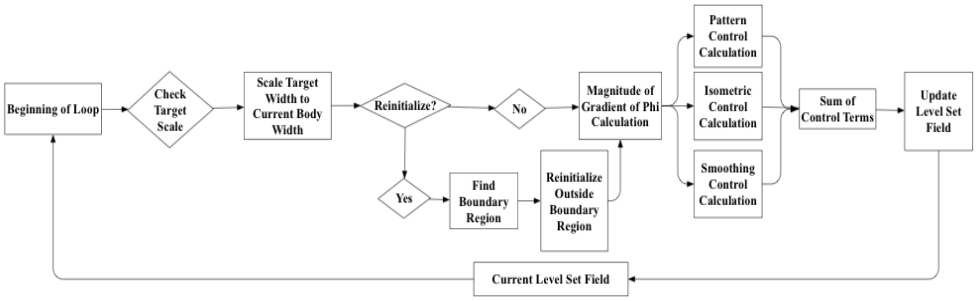


Figure 5: Implementation of primary simulation loop.

Computing $\|\nabla\phi\|$ (labeled Magnitude of Gradient of Phi block in Figure 5) introduces a potential source of numerical error, as derivative operations amplify numerical errors. Therefore, a weak Gaussian filter was introduced in this block to smooth gradient values. The filter uses a two-dimensional Gaussian kernel with a standard deviation of 0.25.

At each step, the surface of the organism ($\phi = 0$) may lie between cells. No attempt is made to interpolate the actual surface (e.g. red contour shown in Figure 6). Rather, figures in this chapter report all cells with $\phi > 0$ as being part of the organism and all cells with $\phi < 0$ as being exterior to the organism.

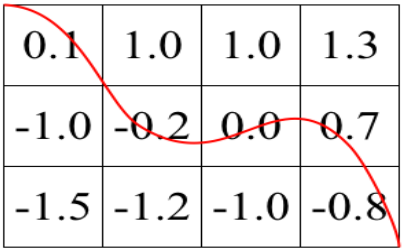


Figure 6: The boundary (red curve) may lie between cell centers, as shown on this grid.

## Section 2.4 Results of Simulation Verification

A suite of four test cases were simulated in order to verify the basic functionality of the algorithm. The four test cases all considered a simulation domain modeling a stereotypical *Xenopus* tadpole tail. The final tail morphology is derived from Reid et. al. [29] and Faber and Nieuwkoop [30]. The four tests include (a) no growth, (b) patterning-based regeneration following amputation, (c) nominal isometric growth, and (d) nominal isometric growth and simultaneous regeneration following amputation. These test cases were selected respectively to examine algorithm stability, performance of patterning control (in isolation), performance of isometric control (in isolation), and performance of combined control terms.

Patterning and isometric control parameters are derived from experimental regeneration data. All four test cases have (unless otherwise noted) $C_{Gc,nom}$ = 0.00075, $C_{\kappa}$ = 0.001, $C_p$ = 0.02, $d$ = 3, $e_{max}$ = 10, $C_{Gc,max}$ = 0.1, 1 time step = 12 minutes, and are run for 15,000 time steps. The patterning control coefficient ($C_p$), was found using the Reid et. al. image sequence and analyzing its length growth rate. Isometric control coefficient ($C_{Gc,nom}$) was found using the normal table of *Xenopus laevis* stage series [30]. The pixel area of the organism was evaluated

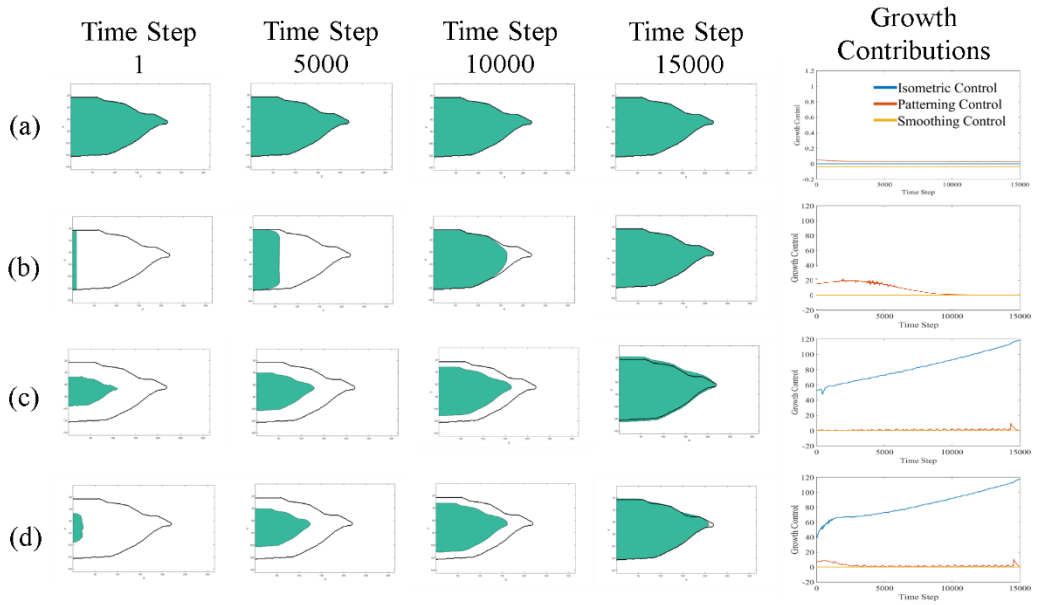


Figure 7: Verification tests: (a) No Growth, (b) Regeneration Following Amputation (c) Nominal Growth (d) Nominal Growth and Simultaneous Regeneration Following Amputation. The right most graph shows contributions of individual control terms to *F*, integrated over the simulation domain.

from experimental images, between stages 40 and 52. Data were plotted and the value of the growth rate was determined by a linear fit of the data.

In analyzing the four test cases, it is useful to consider image sequences that illustrate the growth process. Figure 7 shows four image sequences, one for each test cases. At the end of each row, an additional plot shows growth contributions per time step for each term (P, I, and K). Each image sequence starts from the left; the green body is the current body shape, and the black outline is the final target reference. In the growth contributions plot (far right) the horizontal axis indicates time and the vertical axis indicates the growth contribution (for P, I, and K) integrated over the entire organism for each time step in units. Growth is measured in terms of grid cells, or pixels, that the organism fills. Hence the units

of the vertical axis can be considered to be pixels per unit time. The area under each of the growth contribution curves can loosely be viewed as the overall contribution of material due to each growth contribution (P, I, and K) from the start of the simulation.

### Section 2.4.1 Case A: No Growth

The first test case looks at the stability of the patterning algorithm by considers a fully-grown tail where the surface of the organism is already at its reference location and where the nominal growth term is shut off ($C_{GC,nom} = 0$). One would expect there should be no change in body shape, and little to no contribution from any of the active control regimes, since the initial organism shape matches the reference contour. Indeed, the image sequence in Figure 7(a) shows qualitatively that the tail remains stationary. Growth contributions are tiny but nonzero (smaller than 0.1 pixel/time step, as shown in the growth contributions plot at the end of the row). Though nonzero, the growth contributions from patterning (positive) and smoothing (negative) are essentially balanced. The implication is that the smoothing term is continually active at a low level and that the patterning term compensates, such that the two remain in static equilibrium. The fact that the system reaches equilibrium indicates that the algorithm is in fact stable.

### Section 2.4.2 Case B: Regeneration Following Amputation

The second test case considers a simplified model of regeneration following amputation, with no nominal organism growth. The purpose of the test case is to examine the performance of the patterning control term. The amputation

is performed digitally, with the tail being "cut" at the initial time to leave tissue only in the 10 leftmost grid cells of the image. For this simulation, nominal growth is again disabled ($C_{Gc,nom} = 0$). Under these conditions, we would expect the tail to return its nominal shape (pre-amputation), with tissue filling the reference map much as material might flow into a mold.

Figure 7(b) shows that by time step 15,000, the tail has in fact regenerated to its nominal shape and size. Note that, for Case B only, the patterning growth rate was reduced relative to its nominal value (to $C_p = 0.005$), in order to better visualize the growth process. As shown in the initial sequence, the corners created in the amputation persist through time step 5,000. Together the smoothing term and the reference image (which inhibits patterning growth when the organism boundary reaches the reference boundary) introduce more curvature into the regenerating tail, as seen by time step 10,000. The smoothing term becomes more active as the tail becomes sharper, but eventually the patterning term overcomes the smoothing term to fill the pointed tip of the tail, as seen in time step 15,000.

The growth contribution plot shows that total patterning growth ramps up slowly to a peak around time step 4,000 before tapering toward zero approaching time step 10,000. The explanation is that initially the amputation boundary grows nearly straight (toward the right), such that the total patterning growth (which is proportional to the size of the amputation surface) is nearly constant with some slight rise due to the curvature appearing at the top and bottom corners of the amputated face. As the tail narrows, the surface area of the amputation face grows narrower and the amount of patterning growth falls quickly toward zero. Note that

the scale of the growth contribution plot for Case B is zoomed out by 100 times relative to that of Case A, indicating much, much higher growth rates in Case B (as would be expected).

### Section 2.4.3 Case C: Nominal Growth

The third test case mimics nominal growth with no amputation or regeneration. In this example, the initial organism is set to the same shape as the initial organism in Case A, but scaled down in size by 50%. In concept, one would expect only isometric control would be necessary to grow the tail, even with patterning control active.

The simulation indicates that the organism shape is preserved during growth, as shown in Figure 7(c). The growth contributions plot for this row shows that the majority of all growth is generated by the isometric growth term. Though the patterning growth term is active, it remains essentially zero throughout the simulation, as expected. (The exception is a small spike near time step 15,000, triggered by a combination of the reinitialization process and by erosion due to smoothing). The final image of the sequence shows the simulated organism overgrows the reference contour slightly, as can be observed near the tip of the tail. This occurs largely because of the action of the smoothing term, which rounded the tail during otherwise isometric growth.

As a final note, it is worth observing that the organism growth rate increases slightly over time, as is evident from the growth contributions plot at the end of row (c) in Figure 7. The acceleration of growth over time matches the intent of equation (14), which was designed to keep the rate of cellular division

constant, with the implication that the organisms total growth (pixels added per time step) should become faster as the organism becomes larger.

### Section 2.4.4 Case D: Nominal Growth and Regeneration

A final test case combines Cases B and C to provide a more realistic model for amputation, one in which patterning growth occurs in parallel with nominal growth. For this case, all three control terms are active simultaneously (with control parameters set to their nominal values).

The Case D simulation confirms that the patterning and isometric growth terms complement each other when they are both active, allowing the organism to change size and shape simultaneously. It is perhaps surprising to observe that the combined growth (Case D) image sequence much more closely resembles nominal growth (Case C) than regeneration (Case B). In fact, as early as time step 5000 of the image sequence, Case D and Case C appear qualitatively the same, even though the initial conditions (at time step 1) are entirely different. The similarity of the image sequences can be explained by examining the growth contributions plot, which shows that patterning growth term is most active early, approximately through time step 1000. In fact, the shape of the patterning growth curve for Case D is nearly identical to what was observed for Case B, but with a smaller peak amplitude and scaled to a shorter time scale (about five times faster completion of patterning as compared to Case B). The shortened duration of patterning growth is related to the choice of patterning growth coefficient $C_p$ (which was reduced in Case B) and to the initial condition of Case D (which has

half the width of the initial condition for Case B, such that the velocity-to-length ratio is increased in Case D).

At first glance, it appears that the growth contribution plot for Case D suggests some interaction between the isometric and patterning growth terms, since the isometric growth rate in Case D appears to dip for the first 1000 time steps as compared to Case C. This difference in the initial isometric growth can more simply be explained as a size effect, however, rather than an interaction. Since the total amount of isometric growth scales with the amount of material in the organism, and since the amount of simulated material is very low post amputation (in Case D), it should not be surprising that the volumetric growth rate is initially much lower in Case D than Case C.

## Section 2.5 Discussion

The verification tests described in the prior section, and in particular the Case D test, suggest that this simulation can provide a relevant model for simulation of *Xenopus* regeneration. In the Case D simulation, morphology is regenerated while the tail grows in size, a behavior seen in *Xenopus* regeneration. Importantly, the verification tests of the prior section also demonstrate that the simulation is stable and qualitatively well behaved. The patterning control switches off when the organism shape approaches the reference map (Case A). The isometric growth and volumetric terms perform as expected when active individually (Case B and Case C) and when active simultaneously (Case D). The smoothing control term was active in all cases, providing small adjustments to

regularize shape (as visible in Case B in particular), but always resulting in a very small contribution to the overall growth of the simulated organism, so small that the contribution was only visible when magnifying the scale of the growth contribution plot (as in Case A).

The simulation does have limitations. First, the reinitialization process introduces slight irregularities, since reinitialization occurs only periodically (once every 20 time steps). The result is that the growth contribution plots can appear slightly choppy (as is visible in the saw tooth pattern for patterning growth in Case C and Case D). Reinitialization is also somewhat computationally intensive. As such, an alternative to reinitialization may be pursued in the future. Second, smoothing control effects make it difficult to generate sharp corners. Some modification to the smoothing control may be necessary in the future to allow sharp features to develop when desired (as in the tip of the simulated tail). Third, at small tail sizes, the discrete nature of the patterning control reference map can introduce dithering when the reference map is rescaled. To mitigate this effect, we will consider alternate representations of the reference map in the future. Since, the current reference map is binary (with a one indicating a grid point inside the organism and a zero indicating a grid point outside), a floating point representation of the reference map would likely be helpful to reduce dithering that occurs when the reference map is scaled.

The intended application of our simulation tools is to examine control policies and sensing modalities that might be used during regenerative growth. Future studies will validate our simulation tools through direct comparison to

biological studies of *Xenopus* tail regeneration. Also, we will augment our simulations with new models of control and sensing with the goal of explaining biological observations about the impact of external factors (electrical, chemical, damage, etc.) on regenerative growth.

## Section 2.6 Conclusion

This algorithm creates a simplified abstraction of cell regeneration morphology, using level set methods and control regimes, that is a base module for a future framework to predictively link cell-level signaling to macroscopic patterning. This ultimate framework may provide insight into regeneration, cancer, and even birth defects. This algorithm reduces complex cellular interactions into body boundary movement using three control regimes – patterning control, isometric control, and smoothing control. Patterning control mimics regeneration at wound sites and acts on the body boundary. Isometric control mimics bulk growth of the organism with time, and smoothing control regularizes growth by reducing high curvature regions. Looking specifically at *Xenopus laevis* tail regeneration, this algorithm shows promise in predicting cell patterning on the macroscopic scale. Although this chapter specifically discusses simulation of a *Xenopus* tail in two dimensions, the methodology is general enough to be applied to arbitrary morphologies in both two and three dimensions.

# Chapter 3 A Model for Cell Positioning

## Section 3.1 Introduction

Cell communication and positioning has long been believed to be critical in cellular patterning, growth, and regeneration. Many models have used signaling models to determine cellular gene expression, behavior, and differentiation. Morphogens, signaling chemicals that are transported throughout an organism to alter cell behavior, have long been the focus of this type of research. The simulation presented in this chapter is meant to be a similar type of model that could ultimately provide position estimates to cells in the Chapter 2 simulation. This chapter explores how these morphogens might diffuse throughout a regenerating tail and what their steady state distributions might look like. Recently, *Xenopus laevis* regeneration research has focused on the contribution of voltage potentials, ion concentrations, gap junctions, and signaling pathways to describe how macroscopic patterning may emerge from underlying collaborative phenomena [4], [5], [9], [21], [29], [31], [32]. This simulation could be used to abstract these processes and supply information to "cells" through a diffusion based algorithm.

Nominal regeneration of tadpole tails occurs reliably, and completes, on average, within 14 days of amputation [33]. *Xenopus laevis* can only regenerate its tail and limbs, its body does not have any regenerative ability [34] (unlike *Planaria*), during the early stages of its development. It loses this ability after approximately stage 50 [29]. *Xenopus* tadpole literature classically use an

anterior/posterior and dorsal/ventral coordinate system to describe body feature position. These distinctions can be seen in Figure 8 and are used in this chapter interchangeably with the *x* and *y* axes.

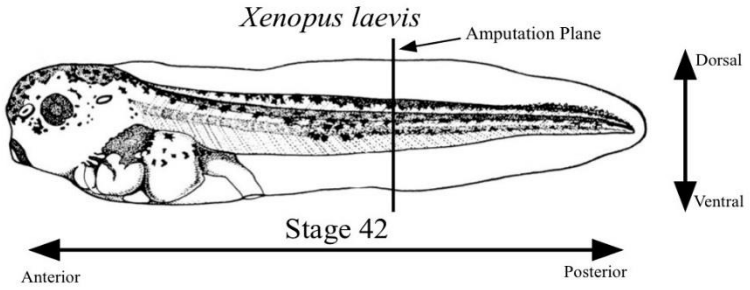


Figure 8: Stage 42 *Xenopus laevis* tadpole with indication of anterior/posterior and dorsal/ventral directions. This image was taken from the Normal Table of Xenopus laevis and is 7.14 mm in length for reference [30].

## Section 3.2 Methods

In this chapter, it is important to note that time steps in the diffusion model are different than time steps in the growth model presented in Chapter 2.Therefore, time steps in the growth model are referred to as "growth time steps" and are much longer than diffusion time steps.

### Section 3.2.1 Diffusion Based Relative Positioning System

The goal of the morphogen model is to abstract the biological mechanism with which cells collectively communicate and position themselves. Cells communicate many ways, including voltage potentials, gap junction pathways, electric fields, and ion concentrations [9], [29], [31], [32], [35], [36] . To mimic this information, a diffusion model, with point sources and a distributed sink, is

proposed. As the morphogen diffuses through the tail, cells destroy it at a regular rate. This process is represented by equation (17)

$$\rho_t = D\rho_{xx} - C\rho + S \tag{17}$$

where, $\rho$ represents the concentration of the morphogen, D is the diffusion coefficient, C is the morphogen rate of destruction and S is the source term. The source cells exist along either the anterior or dorsal edge of the tail and are fixed at a value of one. As the signaling chemical is destroyed, its concentration distribution, when plotted on a log scale, is linear and stable, even as the tail grows (as shown in Figure 9, 10, and 11).

Each of these simulations employs adiabatic boundary conditions on the entire tail boundary. This means no material is allowed to pass through the tail boundaries. As for initial conditions, the source cells are set to one while the rest of the cells are set to zero. The steady state solution is then found iteratively using a discrete Eulerian formulation detailed in the implementation section. The steady state solution is used in this case because it is assumed the morphogen gradient develops much faster than the cells grow.

The steady state solutions to this type of diffusion partial differential equation (equation 17) are exponential in nature. This means the distributions can be more easily visualized as linear when plotted on a logarithmic scale. Figures 9, 10, and 11 employ a logarithmic scale to visualize the steady state distributions of the given morphology. Figure 9 shows the anterior/posterior morphogen distribution of a regenerating tail at 12 days post amputation. The source cells in this case are uniformly distributed along the left edge of the tail image and are highlighted in red. Both Figures 9 and 10 are plotted in the xy plane and have a color bar representing the logarithm of the morphogen concentration.

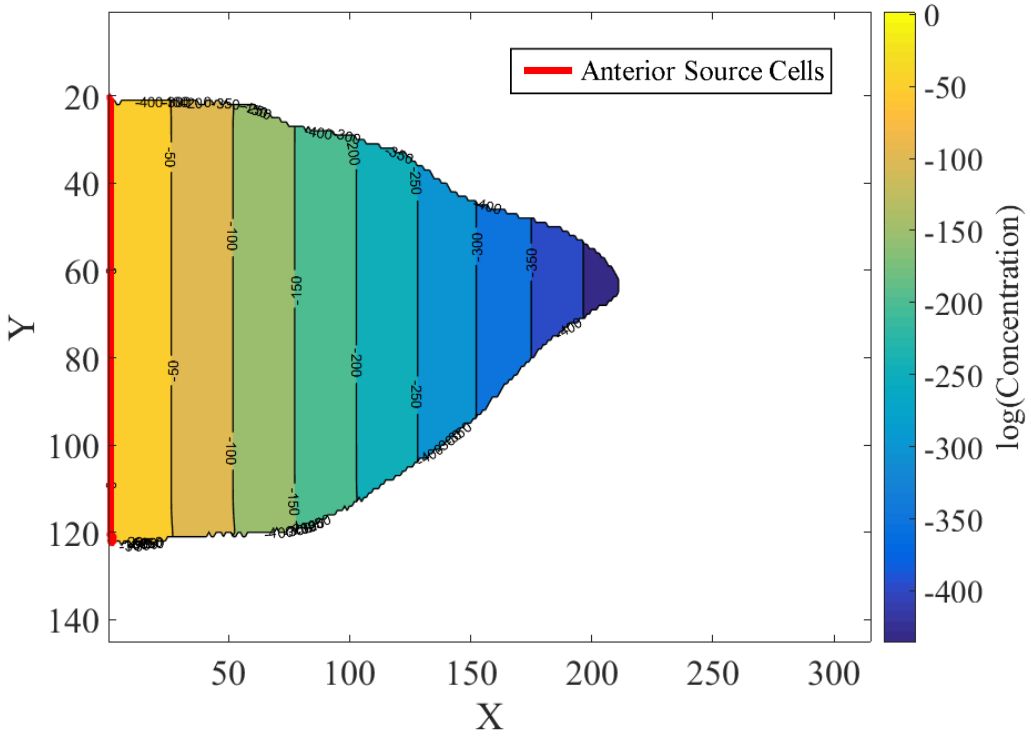


Figure 9: Steady state solution for anterior/posterior morphogen field. Source cells are located along the left edge of the field and highlighted in red.

As can be seen in Figure 9, the steady state solution creates a very evenly spaced distribution and therefore a reliable measure of distance from the souce cells based on concentration.

Similarly to Figure 9, Figure 10 shows the steady state solution to the dorsal/ventral morphogen distribution in a regenerating tail that is 12 days post amputation. The source cells are located along the top (dorsal) edge of the tail and highlighted in pink. The smallest logirathmic term is larger in the dorsal/ventral case because the tail is much longer than it is wide.

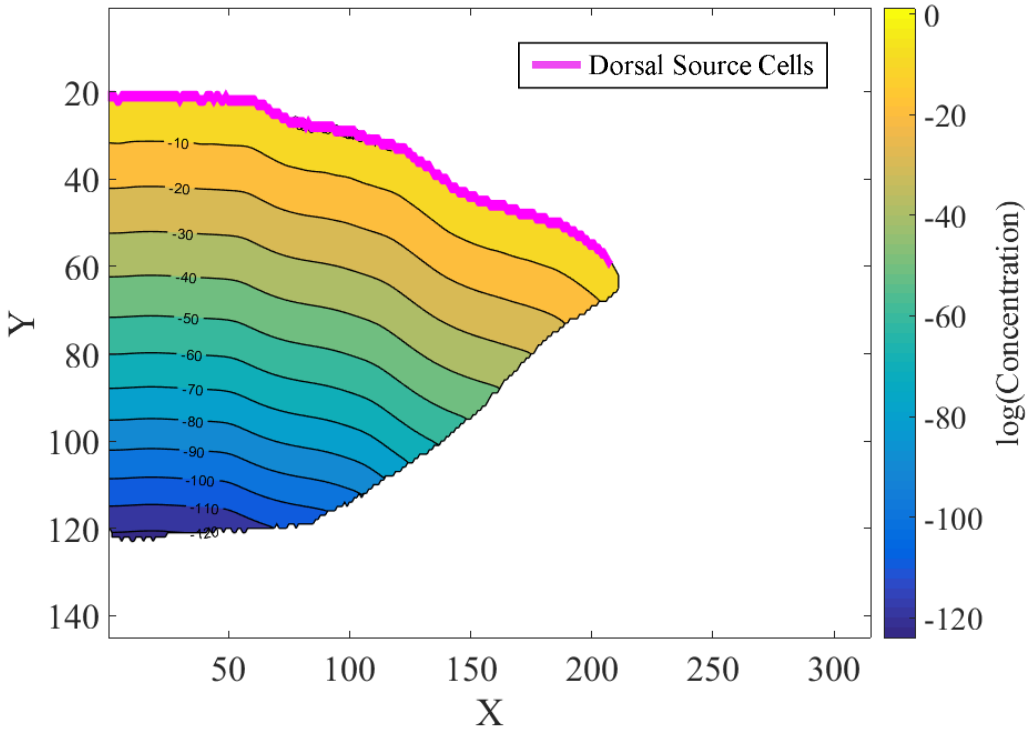


Figure 10: Steady state solution for dorsal/ventral morphogen field. Source cells are located along the top edge of the tail boundary.

Figure 10 exhibits a distribution that is less regular that Figure 9, due to the source cells being placed along an irregular boundary. Although the contours are not as

perfectly distributed, a reliable measure of distance from the dorsal edge can still be extracted from a given concentration.

It is important to note, anterior and dorsal source cells give off different morphogen species, allowing for a unique dorsal/ventral and anterior/posterior position to be found by each cell. Figure (11) shows these two species and the distribution that is formed within an ideal tail section. Figure 11 shows how these morphogen gradients might be used to create a unique coordinate system within the regenerating tail.

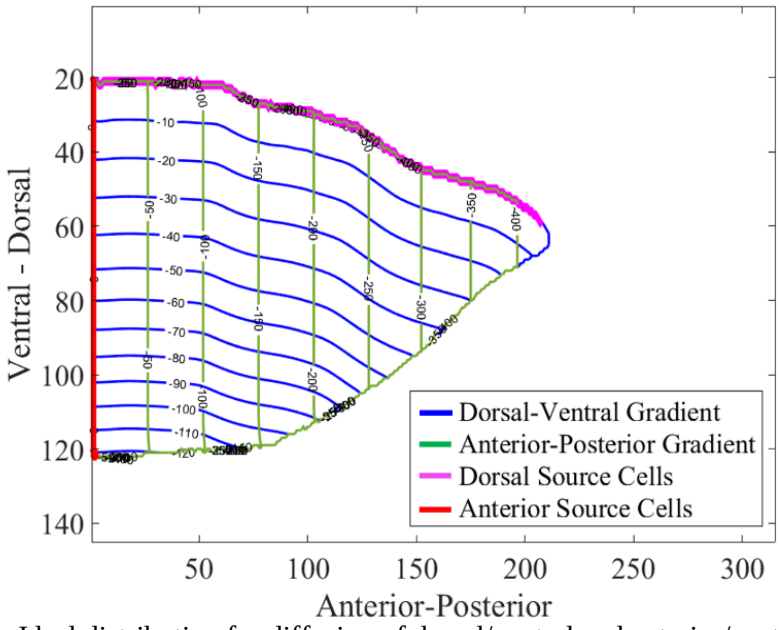


Figure 11: Ideal distribution for diffusion of dorsal/ventral and anterior/posterior chemical species on log scale with D = 0.01, C = 0.01, and dorsal and anterior sources where indicated at 100% concentration.

### Section 3.2.2 Discrete Diffusion Model Formulation

An Eulerian scheme for modeling diffusion was used to generate the concentration distributions. This type of scheme looks at the difference between surrounding grid cells and is shown in equation (18).

$$\frac{\rho^{n+1}(x,y) - \rho^{n}(x,y)}{\Delta t} = D\left(\frac{\rho^{n+1}(x,y+1) - \rho^{n+1}(x,y) + \rho^{n+1}(x,y-1)}{(\Delta x)^2} + \frac{\rho^{n+1}(x+1,y) - \rho^{n+1}(x,y) + \rho^{n+1}(x-1,y)}{(\Delta y)^2}\right) - C\rho^{n+1}(x,y) + S(x,y) \quad (18)$$

In equation (18), ρ is the morphogen concentration, x and y are grid positions, Δt is the time step size, D is the diffusion coefficient, Δx and Δy are the grid step sizes, C is the decay constant, S is the source term, and n denotes the simulation time step.

### Section 3.2.3 Limitations

The major limitation of this method lies in the variability of relation between concentration and distance from source cells as the animal's shape changes. This stems from source cells being located on a section of the animal that is altered as the animal regenerates. Specifically, the source positions along the dorsal edge are not stationary as the tail grows. Another limitation of this simulation is computational intensity increasing with field size. Because the whole field is run to steady state at each growth time step, there is a large computational requirement associated with the use of this module for position estimation.

## Section 3.3 Implementation

This simulation is meant to be a module in the much larger growth and patterning simulation shown in Chapter 2. For this chapter however, the level set growth model and the control scheme will not be used to close the sense-plan-act loop. The results in this chapter show the diffusion system operating from a contour supplied by the level set and control modules working independently. Figure 12 shows the basic implementation architecture used to generate the steady state diffusion solutions. This architecture is run at each growth time step (on the most current zero level set contour) to refresh the steady state solution.

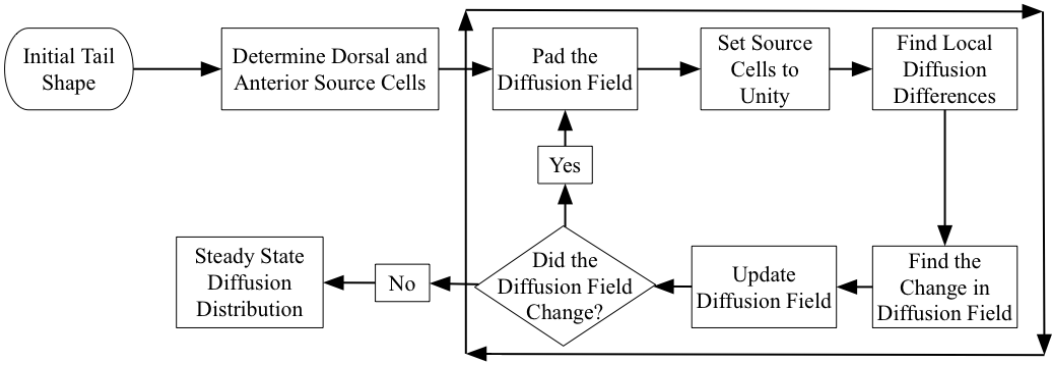


Figure 12: Implementation schematic for the steady state diffusion model.

The implementation shown in Figure 12 starts with an initial tail shape. The initial source positions are then determined from this shape by finding the dorsal and anterior edges of the tail shape. These sources are then initialized to a value of one. An iterative loop is then used to propagate the morphogen until equation (19) is satisfied.

$$|\rho^n - \rho^{n-1}| = 0 \tag{19}$$

Equation (19) is a simple definition of the steady state condition, where the difference between the current time step and the last time step is zero. In simple terms, the field has not changed between time steps. Within the loop, the field is first "padded" on the tail boundary. This means the boundary values are copied one space outside the boundary to create a zero net flux across the boundary (no material is transported at the boundary). The source cells in the field are set to unity – creating material as need. Equations (21a-c) are then used to compute the local differences in the field. These values are then combined in equation (20) to calculate the change in the field with each iteration.

$$\rho_t = \left(D * \Delta t\left(\delta\rho_{right} + \delta\rho_{left} + \delta\rho_{up} + \delta\rho_{down}\right)\right) - C\rho + S \qquad (20)$$

In equation (20), Δt is the time step size, D is the diffusion coefficient, C is the decay coefficient, ρ is the morphogen concentration, S is the source term, and $\delta\rho_{right}$ is the difference between the center and right cell (as shown in equation (21d) and Figure 13). Similarly, $\delta\rho_{left}$, $\delta\rho_{up}$, and $\delta\rho_{down}$ are all differences between the center and their respective cells and are shown in equations (21a-c) and Figure 13.

$$\rho_{up} = \rho(x, y) - \rho(x, y + 1) \qquad (21a)$$

$$\rho_{down} = \rho(x, y) - \rho(x, y - 1) \qquad (21b)$$

$$\rho_{left} = \rho(x, y) - \rho(x - 1, y) \qquad (21c)$$

$$\rho_{right} = \rho(x, y) - \rho(x + 1, y) \qquad (21d)$$

To visualize the local difference shown in equations (21a-d), Figure 13 shows each of these values in relation to a center point ρ(x,y).

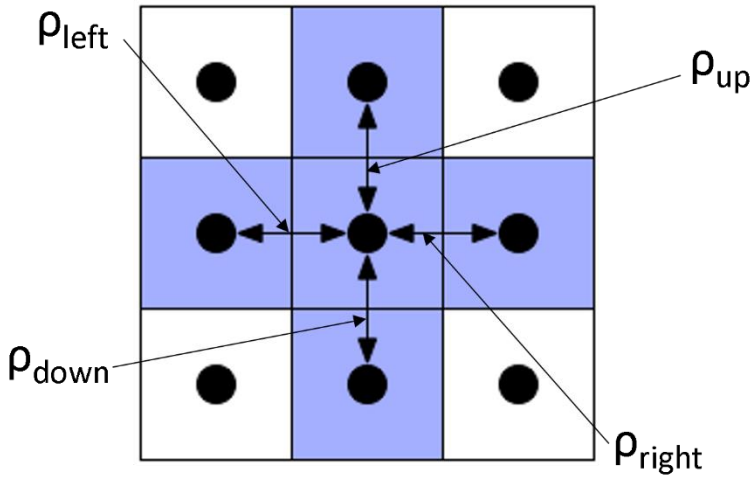


Figure 13: Visualization of Eulerian diffusion scheme. The center point changes at each time step based on equation (20).

To propagate the diffusion scheme in time, the result of equation (20) is used in equation (22).

$$\rho^{n+1} = \rho^n + \rho_t \tag{22}$$

Where n is again the time step and ρ is the morphogen concentration. This process is then repeated until equation (19) is satisfied. At that point, the field has reached its steady state distribution. This process typically takes approximately 2000 time steps for the field shown in Figure 11.

## Section 3.4 Results

This section provides insight into the development of these fields with time. At each growth time step the morphogen distribution is calculated. Figure 14 shows these distributions at four different time steps. The diffusion coefficient

for all sequences is D = 0.01, C = 0.01, and the distributions are run until they reach steady state as explained in the Section 3.3. The left column of Figure 14 shows the anterior/posterior distribution with source cells along the anterior edge of the tail region. The right column shows the dorsal/ventral distribution in the

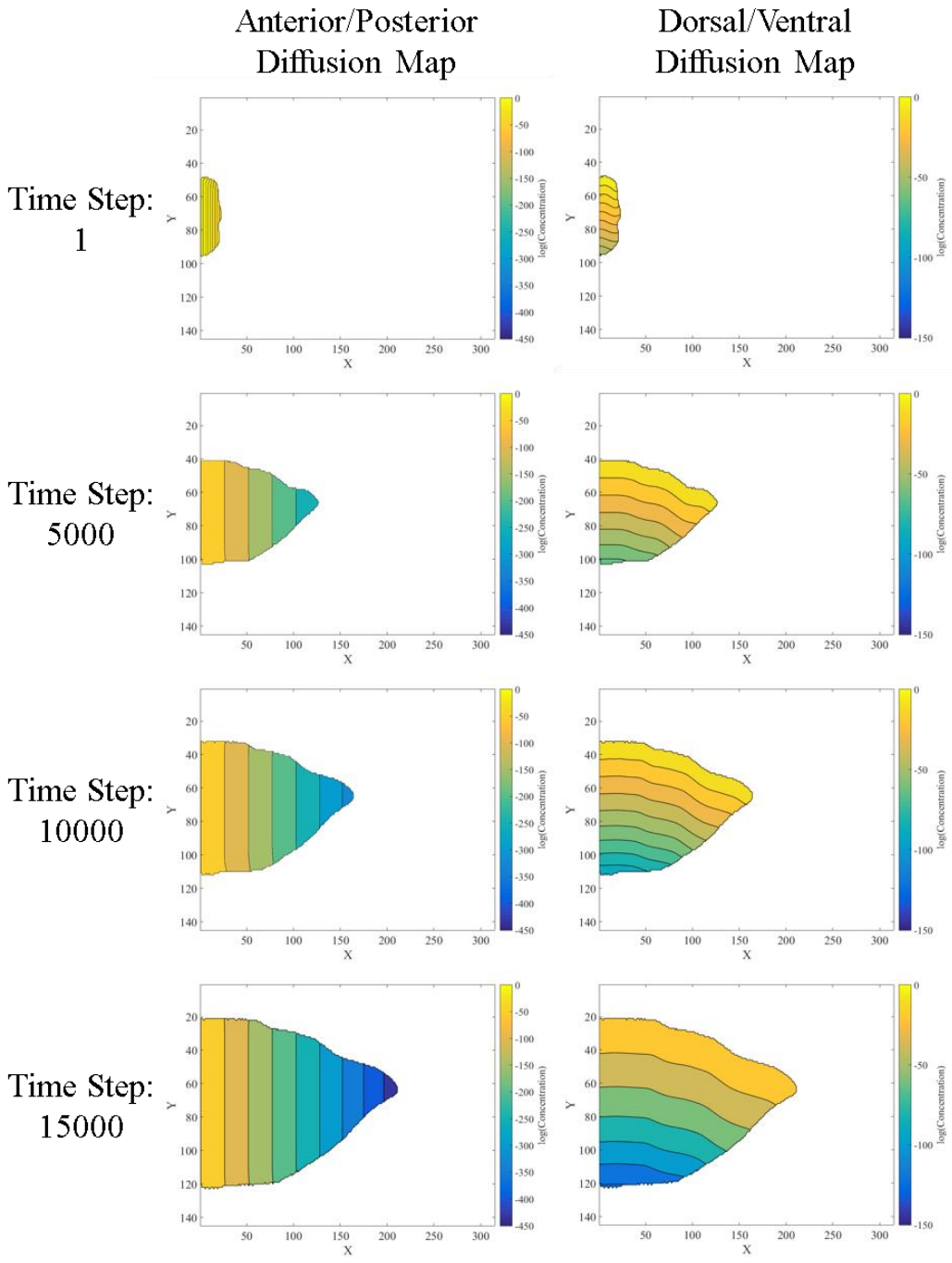


Figure 14: Anterior/Posterior and Dorsal/Ventral diffusion progression in time.

same tail contours. Source cells in this column are distributed along the dorsal edge of the tail. The units on the color bar represents a concentration of 1 molecule per $10^n$ molecules.

These distributions are one possible approach to creating a conformal coordinate system within the growing tail shape. These source locations were largely chosen for their creation of a distribution that aligns closely with the primary coordinate system within the tadpole tail (the anterior/posterior and dorsal/ventral directions). The anterior/posterior distribution directly relates concentration to distance from source cell based on a known distribution. This allows cells to estimate their individual location in the anterior/posterior and dorsal/ventral location.

It is important to note that these two distributions are independent and meant to create unique positions based on a cells value within the two systems (similar to a unique x and y location in a Cartesian coordinate system). The stability in these fields in growth time lend themselves to both cell position estimation and ultimately numerical interpolation to the same coordinate system as the growth and control module. An interpolation step is ultimately required to convert the diffusion position system into Cartesian cell position.

## Section 3.5 Discussion

The results section above shows the progression of the steady state morphogen fields in growth time. The dorsal/ventral and anterior/posterior fields are meant to represent two separate signaling chemicals. This allows for a unique

position to exist for each set of concentration values. As can be seen, the exponential decay, discrete source terms, and adiabatic boundary conditions create a stable concentration field that has a steady state solution. Figure 14 shows this approach scales with tail size effectively and can be used in the future for cell positioning. In figure 14, it is important to note the gradient values shrink with distance from source cells, creating a unique location for each cell in the anterior/posterior and dorsal/ventral fields.

A limitation exists in the biological plausibility of the concentration in the presented plots. The diffusion term D and the decay term C will need to be altered in future simulations to create a minimum concentration, at the largest tail size, of one part per billion. The current minimum is extremely unrealistic at one part per $10^{450}$. Another limitation stems from the instability of source locations in growth time. This causes inconsistent concentration values along the boundaries of the simulation when evaluated in growth time. The steady state solutions are still stable, but as the animal grows the boundary concentrations tend to shift. It is assumed that these gradients develop much faster than cell growth occurs and therefore the diffusion solution needs to be recalculated at each growth time step. The average diffusion solution requires 2000 time steps to converge to steady state and therefore adds a large computational expense to the other components to the overall model detailed in chapter 2. The final limitation in this model stems from its ultimate integration into the control module. The control scheme relies on highly accurate boundary position estimates for the narrow band of patterning control. Because the position estimation model has lower accuracy in the

boundary region it may be an issue in future simulations. This will need to be explored in future work and may be solved by fusing morphogen based positioning estimates and a global positon estimate.

## Section 3.6 Conclusion

This chapter presents and evaluates a diffusion based model that could ultimately be used for estimating cell position based on morphogen concentrations. This type of morphogen model is classically implemented in models of cell differentiation, gene expression, and cell patterning. This particular application, however, uses this morphogen construct to abstract many processes used by cells to communicate and position and ultimately create a relative coordinate system within the tail morphology for cells to estimate their positions. The structure of the diffusion model, with individual source cells and a distribute sink, was shown to have a steady state solution using an iterative Eulerian scheme. This solution also shows stability over multiple tail morphologies. This stability will be crucial for successful integration into the simulation presented in Chapter 2. Two individual morphogen species and corresponding source locations (anterior/posterior and dorsal/ventral species and anterior and dorsal source locations respectively) were used to allow for unique two dimensional locations within the tail morphology. These steady state distributions can directly correlate to a known distance from source cells, making them a plausible cell position estimation mechanism.

# Chapter 4 Conclusion

## Section 4.1 Summary

This thesis introduced a new approach to simulating *Xenopus laevis* tail regeneration. More specifically, it looked at a novel growth simulation, comprised of a level set based physics model and a boundary velocity control scheme, and a model for cell position estimation based on a diffusion model. The simulation modules were introduced to mimic and ultimately predict the regenerative morphology of *Xenopus laevis*. The novel contribution of the thesis is a control scheme that bridges microscopic cell growth and macroscopic tissue patterning.

The growth simulation employed preexisting level set methods to act as a physics model for regenerative growth. A control scheme is implemented on the level set boundary velocity function to mimic microscopic cell operations that ultimately create macroscopic regenerative morphology. The control scheme has three components: patterning control, isometric control, and smoothing control. Patterning control mimics growth in a regeneration bud and alters the morphology of the tail. Isometric control mimics bulk growth of the organism, based on natural cell mitosis and growth, and alters only tail size and not shape. Finally, smoothing control regularizes growth by reducing high curvature regions such as voids or spurs. This methodology shows promise in predicting regenerative morphology. Although *Xenopus laevis* is the focus of this thesis, the methods used in Chapter 2 are general enough to be applied to any two or three dimensional morphology.

The diffusion simulation creates a morphogen distribution based on a classic diffusion equation with discrete sources and a distributed sink. Two morphogen species are independently simulated to create a possible scheme for cell position estimation. The first species is modeled with source cells along the dorsal edge of the tail morphology. The distribution allows cells to relate sensed dorsal/ventral morphogen concentration to distance from the dorsal edge source cells. The second species employs source cells along the anterior most cells in the field and allows cells to relate sensed anterior/posterior morphogen concentration to distance from anterior source cells. These two distributions allow cells to estimate their unique two dimensional position relative to the source cells. This method will ultimately be integrated into the growth model in the future to close the control loop.

This thesis has laid the groundwork for more complex future simulations. Future work focuses on two key aspects. First, the closure of the feedback loop between the navigation and control modules. Second, an analysis of the predictive capability of the simulation by comparing the Case D simulation in Chapter 2 to the real tail regeneration image series.

## Section 4.2 Contribution

This thesis has introduced a set of new control laws to simulate the outer boundary motion of an organism during growth and regeneration.

**Contribution 1: Created a set of novel boundary velocity control laws that link micro-scale cell behavior to macro-scale morphogenesis for use in a simulation of regeneration.**

A model for biological growth and regeneration was created using novel boundary velocity control laws. Level set methods created a field for the boundary motion to take place; while, the control laws manipulate boundary velocities to simulate outer organism boundary motion. This model bridges an existing gap between current micro and macro scale models by abstracting individual cell behavior into collective macroscopic phenomena using the control laws. The model proposed here starts from simple cell behaviors (like mitosis) and merges them with existing level set methods for macro-scale boundary propagation.

Chapter 2 has shown that with the use of the boundary velocity control laws, we have created a viable simulation for biological regeneration. Specifically, Case D in Chapter 2 is able to completely regenerate the tail morphology. These control laws bridge the mesoscale gap and directly link the functions of individual cells to emergent patterning.

*Contribution 1a: Modeled the boundary velocity using three bioinspired control laws: isometric control, patterning control, and smoothing control.*

Three control laws are used in the growth model to mimic key functions during growth and patterning. Patterning control alters tail morphology to regenerate tail shape to mimic regenerative cell growth and patterning. Isometric control alters tail size while preserving shape to mimic natural cell division.

Smoothing control reduces curvature in the field to smooth boundary shape - mimicking the collective cohesiveness of cells. These regimes work in concert to predict regenerative morphology, as shown in Chapter 2.

*Contribution 1b: Simulated Xenopus laevis tail regeneration to test qualitative functionality of proposed control model.*

Four case studies are used to test different control law behaviors and ultimately determine if they qualitatively make sense. In Chapter 2, Case A looks at the stability of patterning control. That case shows it is stable, when at its reference map, and that smoothing control and patterning control balance to ultimately maintain a final shape. Case B looks at patterning control's ability to regenerate morphology, and shows this control law to be operating as expected. Case C demonstrates how isometric control maintains tail shape while altering size (or scale) of the tail. Finally, Case D shows how these control laws can work in concert to regenerate tail morphology post amputation.

Additionally, we published the first paper on modeling regenerative morphology using a level set methodology to disseminate this technique to the broader regenerative and developmental biology community.

**Contribution 2: Evaluated the practicality of a diffusion-based model for cell navigation.**

This module creates two morphogen distributions (Figures 9 and 10) simplify complex cell communication and create unique internal cell positions. Unique dorsal/ventral and anterior/posterior morphogen concentrations can be

sensed and directly linked to these unique cell positions. In the future this model will provide position estimates to the control scheme during regeneration.

## Section 4.3 Future Work

This thesis presents the basic components for a number of future simulations. Two possible avenues for future work are presented below.

### Section 4.3.1 Closing the Feedback Loop

One focus of future work is to close the feedback loop between the navigation module and the control module. The current level set and control modules use ideal positioning information to generate their results. The navigation module can be easily integrated into the overall simulation to substitute position estimates for these ideal positions. This would not only close the loop in this simulation but also allow exploration into what type of positioning information is important for successful regeneration. We would like to explore the relationship between global information, possibly provided by a spine surrogate, and the relative positions created by the morphogen model. This exploration would provide insight into how cells determine position and what information is most important during pattern formation.

### Section 4.3.2 Analysis of Predictive Capability Accuracy

The simulations presented in this thesis are designed to test the overall functionality of the proposed methods but are not directly designed to test predictive capability. We have shown that the individual components of this method function as intended and the simulations are able to regenerate tail

morphology as a whole. What we would like to explore further is the accuracy of the emergent growth rate of the morphology. This rate is collectively created by the interaction of the control laws (which are currently tuned individually using nominal growth and nominal regeneration rates). There is no comprehensive source for all of these parameters and therefore, we would like to create an experimental regeneration image series to determine these values. This will ultimately improve the predictive capability of the Case D simulation presented in Chapter 2.

To create a comprehensive regeneration series, we would like to first perform an actual tadpole amputation and collect a highly detailed series of regeneration images. Currently available regeneration series have ambiguities in scale and growth rate and contain a limited number of samples during a single regeneration. To fix this, a series will ideally be collected that has full body frames, a scaled control frame, a frame of the tadpole pre-amputation, a consistent scale bar, and a large number of sample times (more than 10). This series would allow us to analyze the predictive capability of the simulation in the areas of morphology and growth rate.

There may be differences between experimental and simulation results early in the regeneration process. In an attempt to provide the control scheme with more flexibility during these early time steps, we would like to explore varying the patterning control formulation in one of two way. The first possibility is to delay the onset of patterning control until later in the simulation. The second possibility is to vary the patterning boundary layer thickness. Before we can test either of

these possibilities however, we will first need to create the regeneration series to compare them with.

# References


[1] B. C. Thorne, A. M. Bailey, D. W. DeSimone, and S. M. Peirce, "Agent-based modeling of multicell morphogenic processes during development," *Birth Defects Res. Part C Embryo Today Rev.*, vol. 81, no. 4, pp. 344–353, Dec. 2007.

[2] J. Green, "Morphogen gradients, positional information, and Xenopus: Interplay of theory and experiment," *Dev. Dyn.*, vol. 225, no. 4, pp. 392–408, Dec. 2002.

[3] N. Bessonov, M. Levin, N. Morozova, N. Reinberg, A. Tosenberger, and V. Volpert, "On a Model of Pattern Regeneration Based on Cell Memory," *PLOS ONE*, vol. 10, no. 2, Feb. 2015.

[4] A. Tseng and M. Levin, "Cracking the bioelectric code," *Commun. Integr. Biol.*, vol. 6, no. 1, Jan. 2013.

[5] M. Levin, "Morphogenetic fields in embryogenesis, regeneration, and cancer: non-local control of complex patterning," *Biosystems*, vol. 109, no. 3, pp. 243–261, Sep. 2012.

[6] D. C. Walker, G. Hill, S. M. Wood, R. H. Smallwood, and J. Southgate, "Agent-based computational modeling of wounded epithelial cell monolayers," *IEEE Trans. NanoBioscience*, vol. 3, no. 3, pp. 153–163, Sep. 2004.

[7] M. Hwang, M. Garbey, S. A. Berceli, and R. Tran-Son-Tay, "Rule-Based Simulation of Multi-Cellular Biological Systems—A Review of Modeling Techniques," *Cell. Mol. Bioeng.*, vol. 2, no. 3, pp. 285–294, Aug. 2009.

[8] P. V. Liedekerke, M. M. Palm, N. Jagiella, and D. Drasdo, "Simulating tissue mechanics with agent-based models: concepts, perspectives and some novel results," *Comput. Part. Mech.*, vol. 2, no. 4, pp. 401–444, Nov. 2015.

[9] D. Lobo and M. Levin, "Inferring Regulatory Networks from Experimental Morphological Phenotypes: A Computational Method Reverse-Engineers Planarian Regeneration," *PLOS Comput. Biol.*, vol. 11, no. 6, Jun. 2015.

[10] V. Manca and G. Pardini, “Morphogenesis through moving membranes,” *Nat. Comput.*, vol. 13, no. 3, pp. 403–419, Jan. 2014.

[11] E. Bianconi, A. Piovesan, F. Facchin, A. Beraudi, R. Casadei, F. Frabetti, L. Vitale, M. C. Pelleri, S. Tassani, F. Piva, S. Perez-Amodio, P. Strippoli, and S. Canaider, “An estimation of the number of cells in the human body,” *Ann. Hum. Biol.*, vol. 40, no. 6, pp. 463–471, Dec. 2013.

[12] K. A. Rejniak and A. R. A. Anderson, “Hybrid models of tumor growth,” *Wiley Interdiscip. Rev. Syst. Biol. Med.*, vol. 3, no. 1, pp. 115–125, Jan. 2011.

[13] J. A. Sethian, “Curvature and the evolution of fronts,” *Commun. Math. Phys.*, vol. 101, no. 4, pp. 487–499, Dec. 1985.

[14] S. Osher and J. A. Sethian, “Fronts propagating with curvature-dependent speed: Algorithms based on Hamilton-Jacobi formulations,” *J. Comput. Phys.*, vol. 79, no. 1, pp. 12–49, Nov. 1988.

[15] J. Sethian, “Turbulent combustion in open and closed vessels,” *J. Comput. Phys.*, vol. 54, no. 3, pp. 425–456, Jun. 1984.

[16] J. A. Sethian, *Level Set Methods: Evolving Interfaces in Geometry, Fluid Mechanics, Computer Vision, and Materials Science*. Cambridge Monographs on Applied and Computational Mathematics.

[17] C.S. Hogea, B. T. Murray, and J. A. Sethian, “Simulating Complex Tumor Dynamics from Avascular to Vascular Growth using a General Level Set Method,” *J. Mathmatical Biol.*

[18] M. Suzuki, N. Yakushiji, Y. Nakada, A. Satoh, H. Ide, and K. Tamura, “Limb Regeneration in *Xenopus laevis* Froglet,” *Sci. World J.*, vol. 6, pp. 26–37, 2006.

[19] K. Friston, M. Levin, B. Sengupta, and G. Pezzulo, “Knowing one’s place: a free-energy approach to pattern regulation,” *J. R. Soc. Interface*, vol. 12, no. 105, p. 20141383, Apr. 2015.

[20] Y. Zhang and M. Levin, “Particle Tracking Model of Electrophoretic Morphogen Movement Reveals Stochastic Dynamics of Embryonic Gradient,” *Dev. Dyn.*, no. 238, pp. 1923–1935, 2009.

[21] B. T. Chernet, C. Fields, and M. Levin, “Long-range gap junctional signaling controls oncogene-mediated tumorigenesis in Xenopus laevis embryos,” *Biophysics*, vol. 5, p. 519, 2015.

[22] D. Lobo, M. Solano, G. A. Bubenik, and M. Levin, “A linear-encoding model explains the variability of the target morphology in regeneration,” *J. R. Soc. Interface*, vol. 11, no. 92, p. 20130918, Mar. 2014.

[23] P. K. Kundu, I. M. Cohen, and David R. Dowling Ph.D., *Fluid Mechanics*, 5th Edition. Academic Press, 2011.

[24] K. A. Brakke, *The Motion of a Surface by Its Mean Curvature. (MN-20)*. Princeton University Press, 2015.

[25] L. C. Evans and J. Spruck, “Motion of Level Sets by Mean Curvature. I,” *J Differ. Geom.*, vol. 33, no. 3, pp. 635–681, 1991.

[26] R. S. King and P. A. Newmark, “The cell biology of regeneration,” *J. Cell Biol.*, vol. 196, no. 5, pp. 553–562, Mar. 2012.

[27] D. Lobo, W. S. Beane, and M. Levin, “Modeling Planarian Regeneration: A Primer for Reverse-Engineering the Worm,” *PLoS Comput Biol*, vol. 8, no. 4, p. e1002481, Apr. 2012.

[28] N. R. Love, Y. Chen, S. Ishibashi, P. Kritsiligkou, R. Lea, Y. Koh, J. L. Gallop, K. Dorey, and E. Amaya, “Amputation-induced reactive oxygen species are required for successful Xenopus tadpole tail regeneration,” *Nat. Cell Biol.*, vol. 15, no. 2, pp. 222–228, Feb. 2013.

[29] B. Reid, B. Song, and M. Zhao, “Electric currents in Xenopus tadpole tail regeneration,” *Dev. Biol.*, vol. 335, no. 1, pp. 198–207, Nov. 2009.

[30] J. Faber and P. D. Nieuwkoop, *Normal table of Xenopus laevis (Daudin) : a systematical and chronological survey of the development from the fertilized egg till the end of metamorphosis*, 2nd ed. Amsterdam : North-Holland Pub. Co, 1967.

[31] C. Gargioli and J. M. W. Slack, “Cell lineage tracing during Xenopus tail regeneration,” *Development*, vol. 131, no. 11, pp. 2669–2679, Jun. 2004.

[32] M. Levin, “Bioelectric mechanisms in regeneration: Unique aspects and future perspectives,” *Semin. Cell Dev. Biol.*, vol. 20, no. 5, pp. 543–556, Jul. 2009.

[33] M. Mochii, Y. Taniguchi, and I. Shikata, “Tail regeneration in the Xenopus tadpole,” *Dev. Growth Differ*, no. 49, pp. 155–161, 2007.

[34] S. Filoni and L. Bosco, “Comparative analysis of the regenerative capacity of caudal spinal cord in larvae of serveral Anuran amphibian species,” *Acta Embryol. Morphol. Exp. Halocynthia Assoc.*, vol. 2, no. 3, pp. 199–226, Jan. 1981.

[35] D. V. Krysko, L. Leybaert, P. Vandenabeele, and K. D’Herde, “Gap junctions and the propagation of cell survival and cell death signals,” *Apoptosis*, vol. 10, no. 3, pp. 459–469, May 2005.

[36] M. J. Sanderson, A. C. Charles, S. Boitano, and E. R. Dirksen, “Mechanisms and function of intercellular calcium signaling,” *Mol. Cell. Endocrinol.*, vol. 98, no. 2, pp. 173–187, Jan. 1994.